

The mass distribution in the innermost regions of Spiral Galaxies.

Charu Ratnam & Paolo Salucci

*International School for Advanced Studies, SISSA, Via Beirut 2-4, I-34013
Trieste, Italy*

Abstract

We use high-spatial resolution (~ 100 pc) rotation curves of 83 spiral galaxies to investigate the mass distribution of their innermost kpc. We show that, *in this region*, the luminous matter completely accounts for the gravitational potential and no dark component is required. The derived I-band disk mass-to-light ratios \mathcal{Y}_I agree well with those obtained from population synthesis models and correlate with color in a similar way. We find strict upper limits of $\sim 10^7 M_\odot$ for the masses of compact bodies at the center of spirals, ruling out that these systems host the remnants of the quasar activity.

1 Introduction

There is increasing direct evidence that, at the centers of bulge-dominated galaxies there reside Massive Dark Objects (MDO), which are probably the remnants of the engines that once powered the QSO phenomenon (Ho, 1998; Kormendy & Richstone, 1995). In fact, virtually every hot galaxy hosts a MDO/BH with a mass ranging from $\sim 10^8 M_\odot$ to $2 \times 10^{10} M_\odot$, similar to those related to the QSO phenomenon. For disk galaxies, the situation is different and much more uncertain. A direct determination of the central mass has been obtained only in very few cases which include our own Galaxy where a black hole with a mass $2 \times 10^6 M_\odot$ has been discovered (Ghez et al. 1999, Genzel 1998; see also Salucci et al 1999 for other few cases). Remarkably, these masses do not exceed $10^7 M_\odot$; however, the lack of detections of very massive objects ($M_{MDO} > 10^8 M_\odot$) cannot be ascribed to observational biases. In fact, the rotation curves (RC), in great number available down to $r_{in} \sim 100$ pc, could easily expose central bodies with masses of the order of $\sim 10^8 M_\odot$, given that usually $V(r_{in}) \sim 10$ km/s, or equivalently, the stellar mass inside 100 pc barely reaches $10^7 M_\odot$. On the other hand, the same RC analysis determining the MDO mass, obtain also the mass distribution of the innermost regions. This

is particularly important in the case of low luminosity DM-dominated spirals (see Persic and Salucci, 1990) for which it is generally difficult to disentangle the disk component from the whole bulk of gravitating matter. In any cases, let us stress that to properly model the region where the luminous matter dominates is indispensable to infer the structural properties of dark matter.

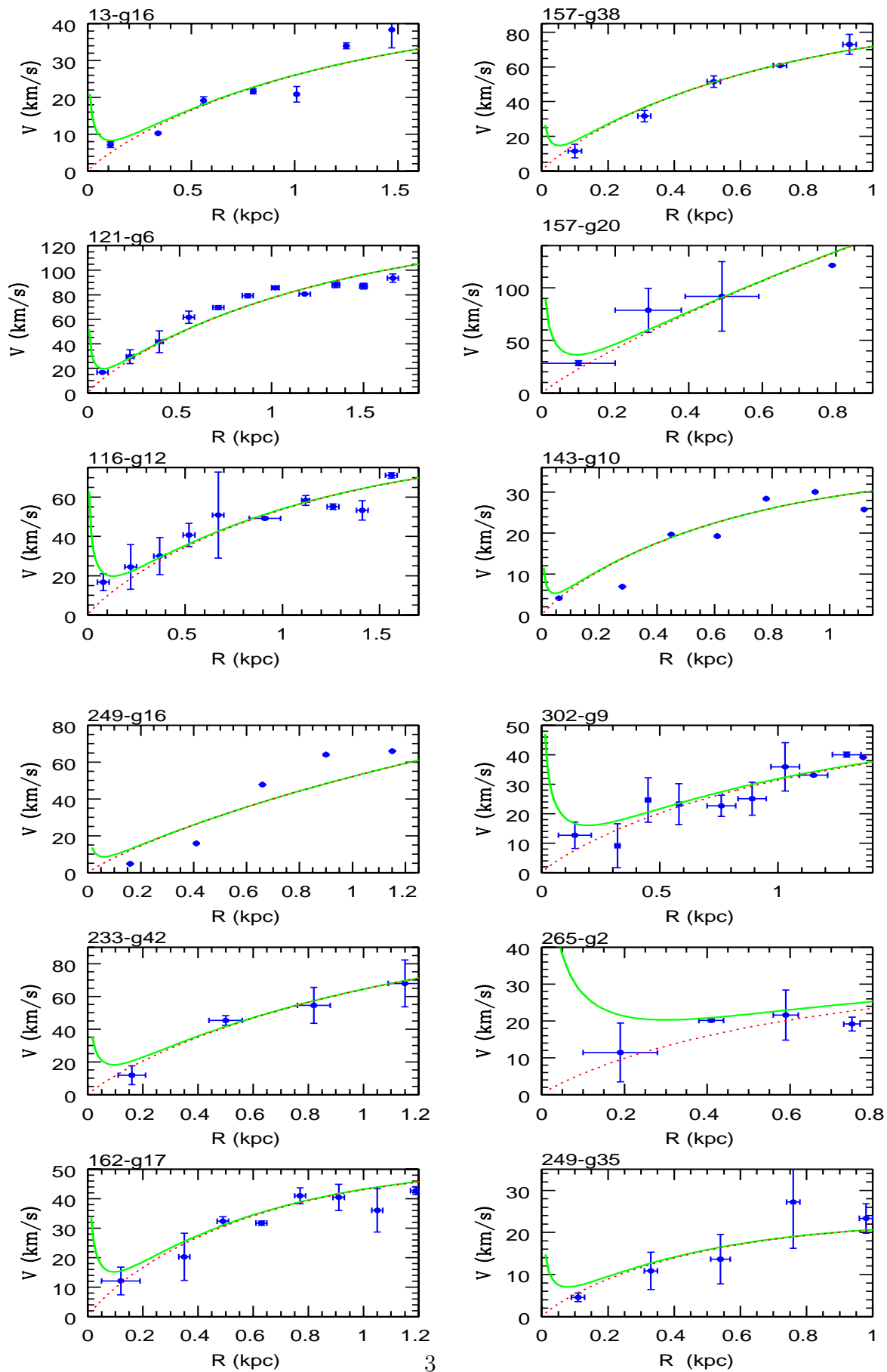
The aim of this work is to study the innermost kinematics of spirals in order to *a)* investigate the distribution of matter in relation to that of light *b)* set stringent upper limits on the MDO masses. The plan of the paper is the following: in section 2 we analyse a sample drawn from the 967 rotation curves (RC's) of Persic and Salucci (1995), in section 3 we derive and discuss the disk properties and in sections 4 and 5 we derive upper limits on the MDO/BH masses and discuss the results. In this paper we assume $H_0 = 75 \text{ km/s Mpc}^{-1}$, and take, as the reference magnitude in the B-band, $M_* = -20.5$, which translates to $M_* - 21.9$ in the I-band (e.g. Rhee, 1997). All luminosities correspond to the I-band unless otherwise specified.

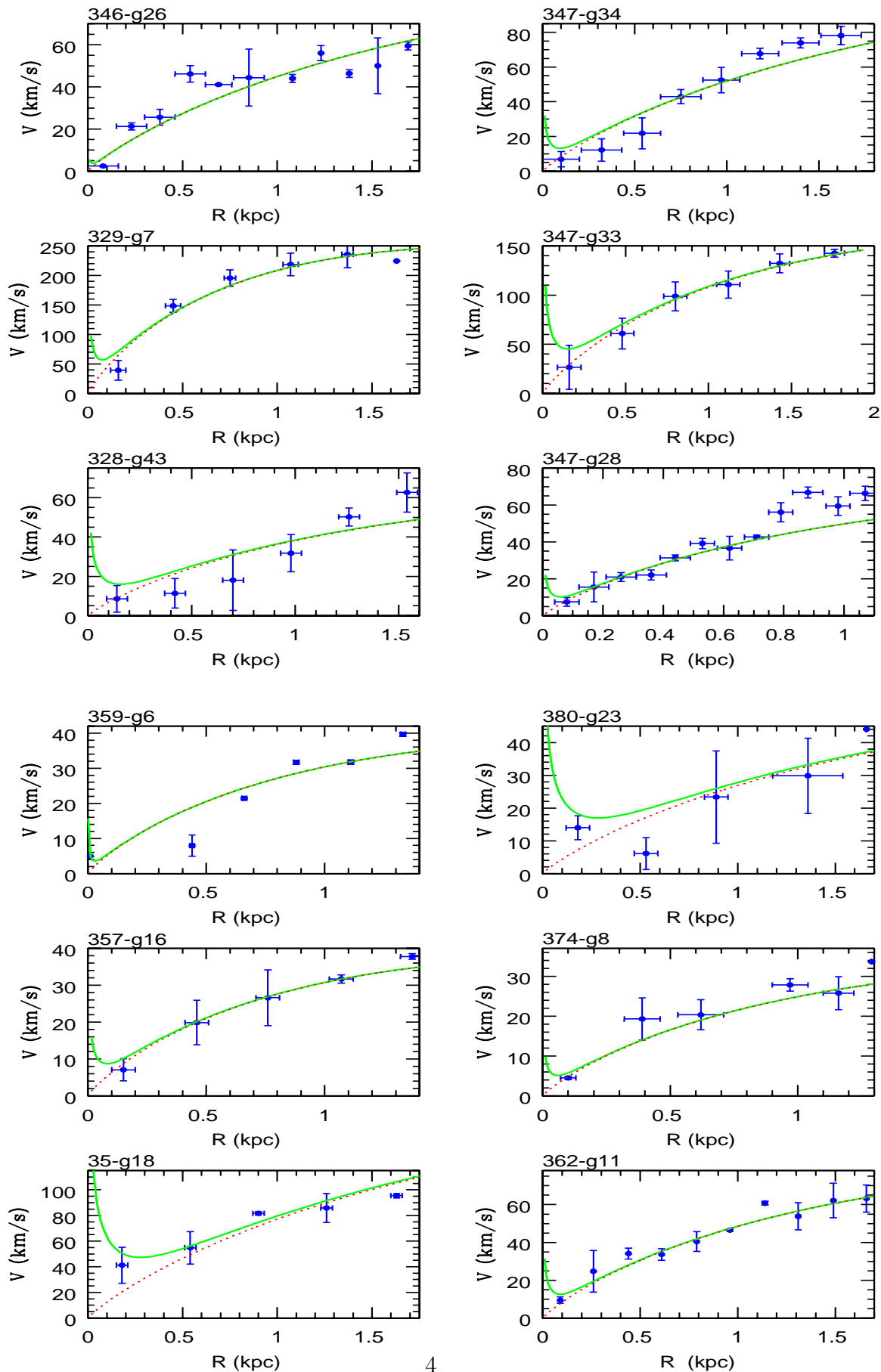
2 Inner Rotation Curves of Late Types Spirals and mass modeling

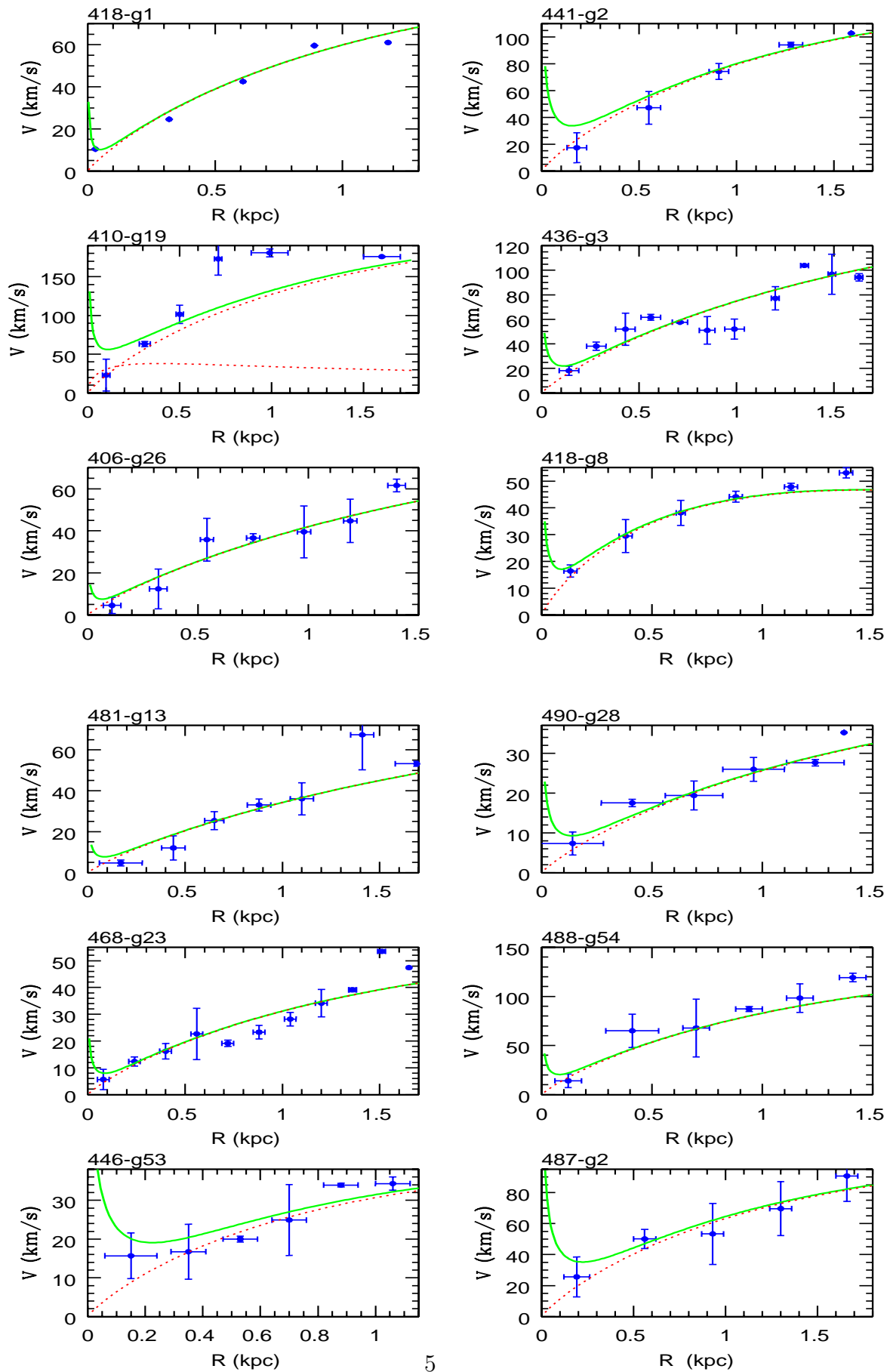
Recently, about a thousand rotation curves of spiral galaxies (PS95), tracing the kinematics inside the central kpc, have been available. Among these, about one hundred have at least one measurement $< 200 \text{ pc}$ and several $< 500 - 1000 \text{ pc}$. For these objects the detection of a MDO of $\sim 10^8 M_\odot$ or more, if present, is guaranteed and so is the determination of the stellar disk mass, provided that in this region the stellar disk is the major mass component.

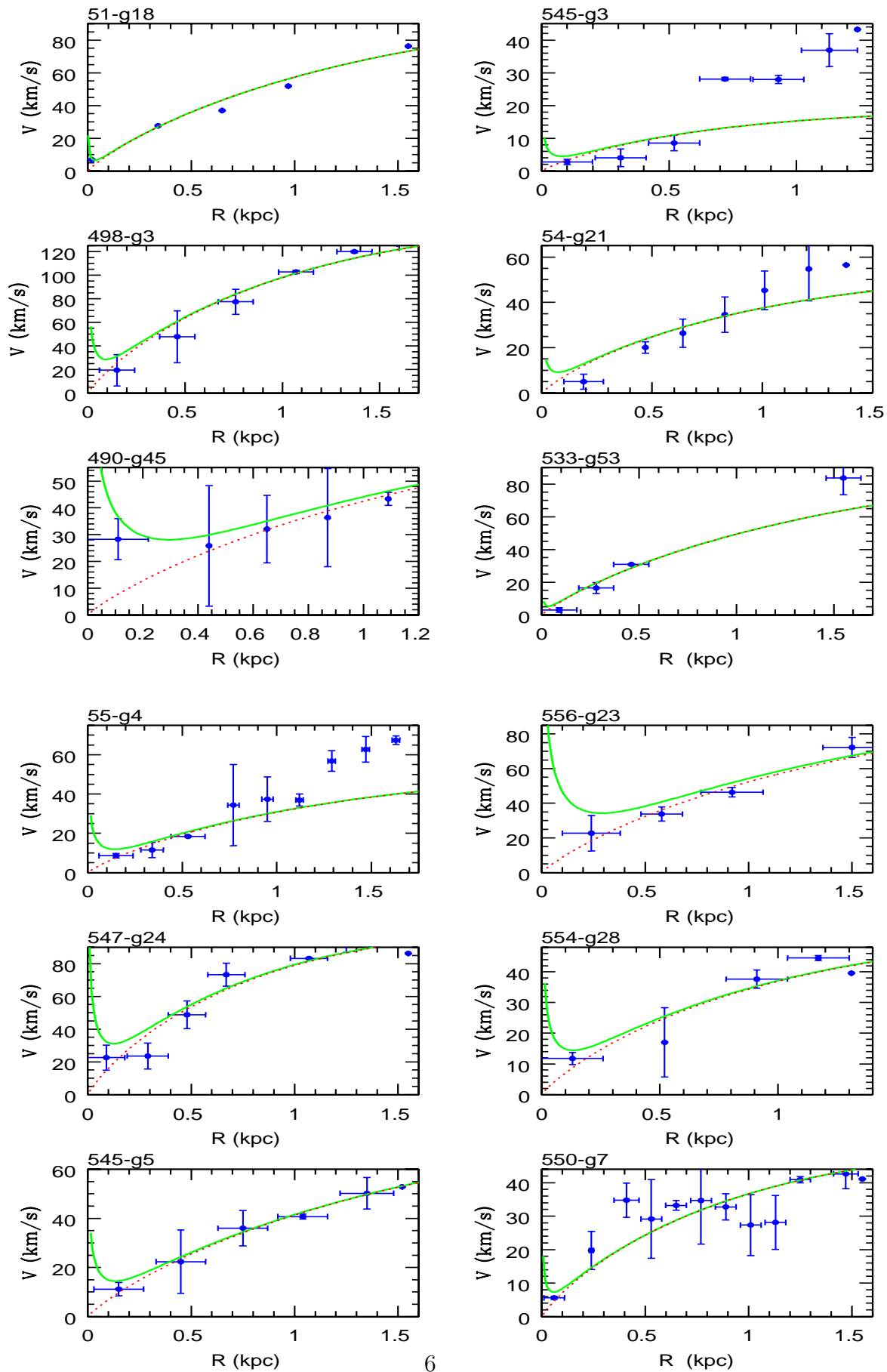
Therefore, we select from PS95 the largest sample of rotation curves equally distributed in magnitude interval and of sufficient high-quality for our purposes, by setting the following criteria: *i)* each RC has at least 4 measurements inside a radius of $340(1 - \frac{(M_I+15)}{9}) \text{ pc} \sim (350 - 500) \text{ pc}$, *ii)* for each RC, the innermost data is situated at a radius $r_{in} < 100(1 - \frac{(M_I+15)}{18}) \sim (100 - 150) \text{ pc}$. Let us notice that to restrict the criteria reduces the number of RC's without improving their already high quality that however rapidly decreases as they are relaxed. The rotation curves resulting from the selection are generally smooth, axisymmetric and with negligible non circular perturbations. It is evident that there is a very good agreement between the rotation fields on the receding and the approaching arm (see PS95). The sample (Sample B in Salucci et al., 2000) has 83 objects, well mixed in luminosity and almost equally distributed between Sb-Sc and Sd-Im Hubble types.

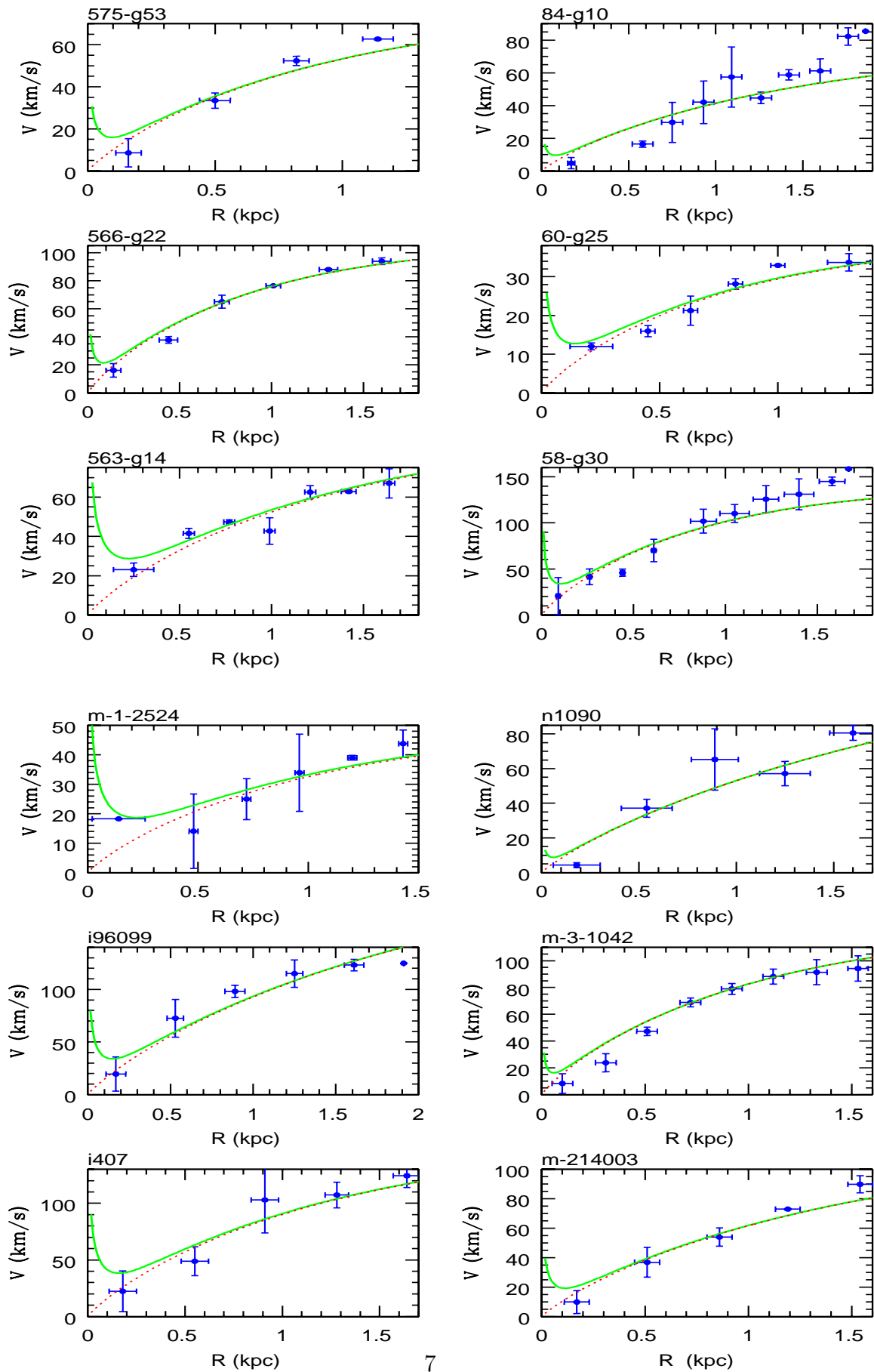
We aim to reproduce the RCs by a mass model featuring: (*i*) a Freeman disk of length-scale R_D , (derived in PS95) and mass M_D , which contributes to the

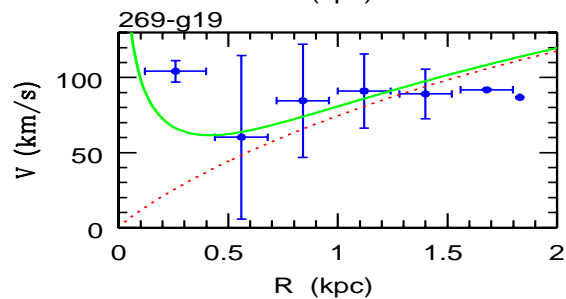
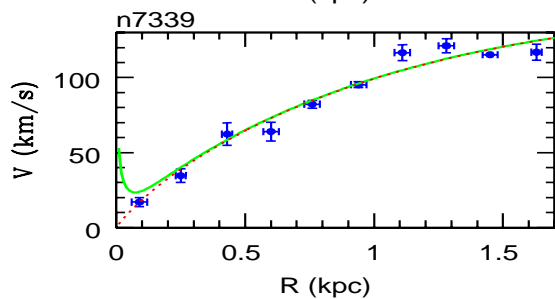
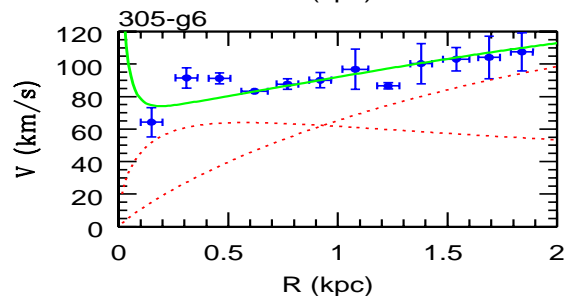
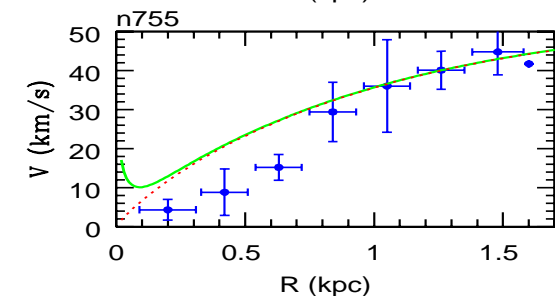
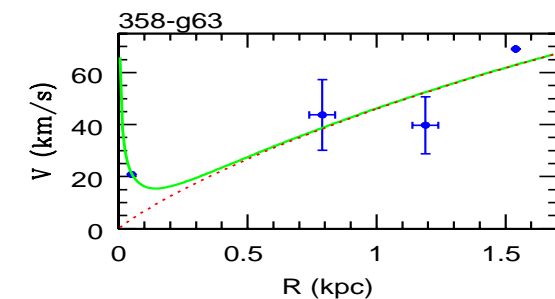
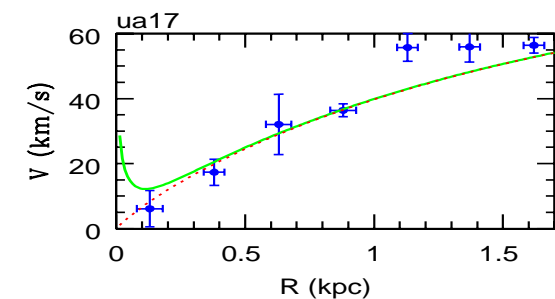
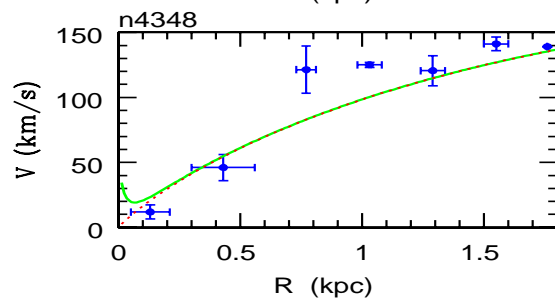
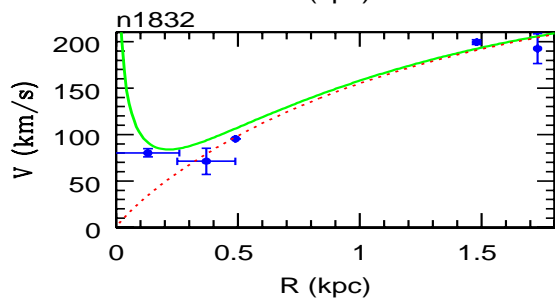
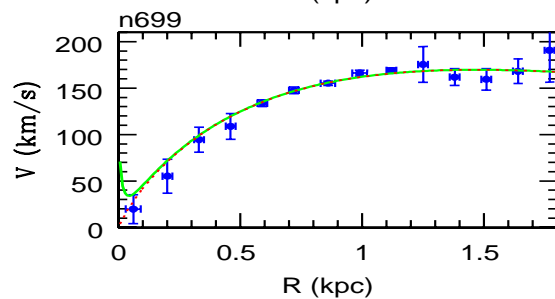
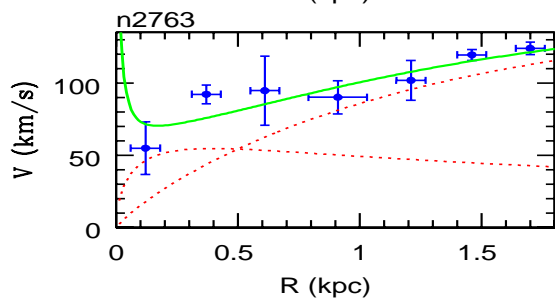
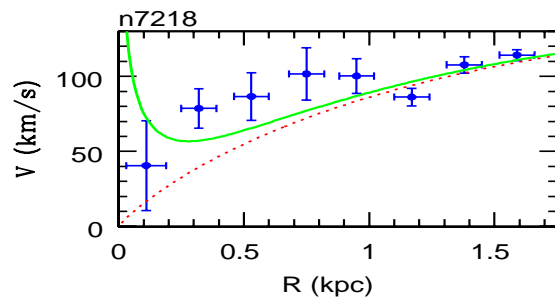
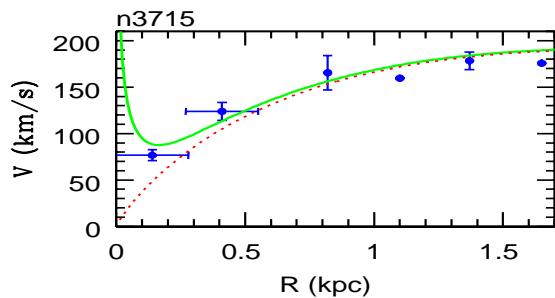












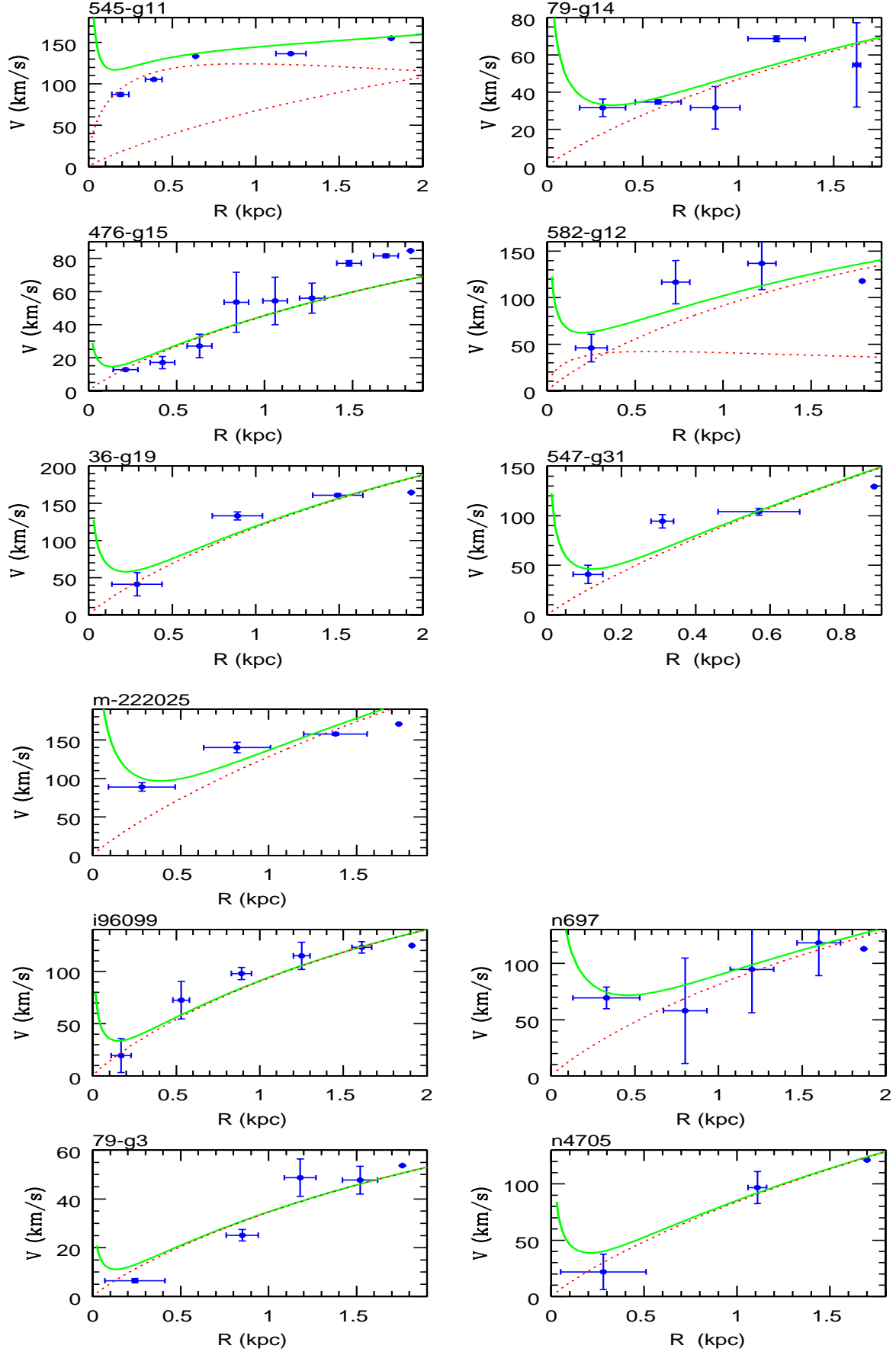


Fig. 1. Mass models of the 83 objects of sample B. The dashed lines indicate the OD model (in a few cases a bulge has been included) while the solid line indicates the disk+BH model.

circular velocity as:

$$V_d^2(R) = \frac{1}{2}GM_D/R_D x^2(I_0K_0 - I_1K_1)_{x/2} \quad (1)$$

where I_n, K_n are modified Bessel functions and $x = R/R_D$, and (ii) a MDO which contributes to $V(R)$ as:

$$V_{MDO}^2(R) = GM_{MDO}/R \quad (2a)$$

where the MDO mass is:

$$M_{MDO} = fG^{-1}V^2(r_{in})r_{in} \quad (2b)$$

with $0 < f \leq 1$.

In Fig.(1) we compare the velocity data with the best-fitting mass models in the cases of 1) $f = 0$ (only disk, OD) mass model and of 2) $f > 0$ (disk+ black hole) mass model (in practice: $f \simeq 1$). As result, we find no central-body-dominated (CBD) rotation curve, i.e. no RC shows the Keplerian fall-off expected for a CBD RC. On the contrary, rotation curves are strikingly close to those predicted by the OD model, i.e. by a self-gravitating exponential thin disk with radially constant mass-to-light ratio. The results of the mass modeling are: in 57 objects the OD velocity curve accounts for the rotation data in a *excellent* way and it lies within the data error bars (for $R < R_{IBD}$ see below). In 14 cases¹ the luminous matter accounts for the rotation curve in a *satisfactory* way: data and model differ utmost by 2σ and no evidence for an additional component emerges. In 9 cases² the OD fits are *reasonable* especially if we consider that the corresponding RC's have non-negligible internal dispersion and/or some asymmetry. The low-luminosity galaxy 545-G3 is dominated by dark matter at any radius. Finally, in 2 cases; 346-G26, 410-G19, the OD model reproduces the data with some difficulty.

A simple inspection of the results shows that in every galaxy only for $R \geq R_{IBD}$ ³ the dark component begins to significantly contribute to the total gravitational potential. We then confirm the picture of Salucci & Persic (1999) and Salucci et al, (2000) according to which, the luminous matter dominates an innermost region of spirals of size R_{IBD} . This truly baryonic scale turns out to be a function of galaxy luminosity by ranging from $0.5R_D \sim 0.5kpc$ to $2R_D \sim 30kpc$ along the luminosity sequence. Such a transition can be seen, e.g. in the RC of 55-G4: OD curve reproduces the data only out to $R = R_{IBD} \sim 0.5kpc$. More in general, the best-fit models (see Fig 1) clearly

¹ 349-G6, 38-G23, 35-G18, 157-G20, 436-G3, 468-G23, 547-G24, 550-G7, N4348, 358G-63, 582-G12, 547-G31, I96099, N4705

² 347-G84, 328-G43, 249-G16, 84-G10, N755, 79-G14, M222025, N7218, 249-G16

³ Inner Baryon Dominance

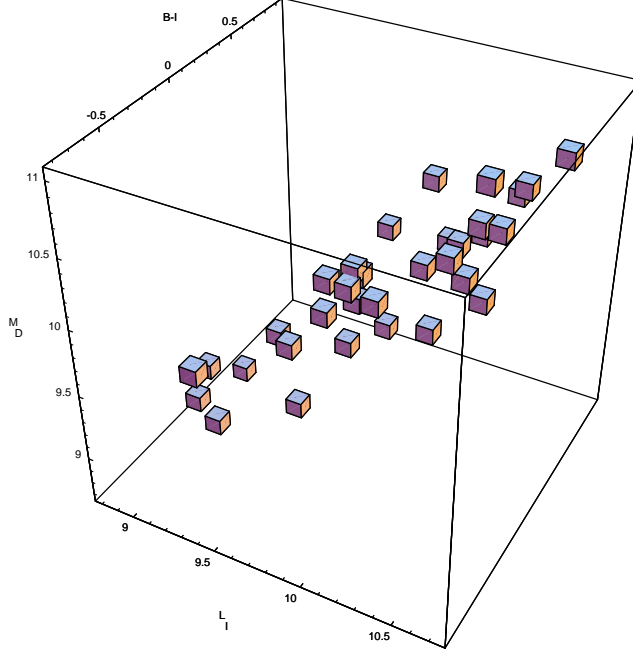


Fig. 2. The 3D space of galaxy properties. $M_D - (B - I) - L_I$.

show that, with the exception of the least luminous galaxy, at $R \sim 0.5 \text{ kpc}$, the DM contribution to the RC lies below the detection threshold. On the other hand, in order to become the major component at a $2 - 3$ disk scale-lengths, the dark mass, negligible at 0.5 kpc must *strongly* increase with radius.

We conclude by stating that the OD mass models reproduce the innermost kpc of the rotation curves extremely well: on this scale, there is no hint of a dark component.

3 Disk properties

Disk masses are derived from eq (1); Although the uncertainties on the *disk* mass-to-light ratio values must include model-fit uncertainties, photometry errors, and uncertainties on the assumed inclination and distance (the latter present also for Tully-Fisher distances). The uncertainty budget can be roughly estimated as: $\delta M_D / L_I \simeq 0.4 M_D / L_I$.

The present sample of DM-free mass models is a most suitable one for investigating the disk masses in relation with the photometric properties of galaxies. In detail, this is done with a sub-sample of Sample B comprising 28 objects for which I -band luminosities and $B - I$ colors are available. In Table 1 we report best-fit disk masses, color, mass-to-light ratios M_D / L_I and luminosity for these objects. $B-I$ color are good indicators of stellar mass-to-light ratio

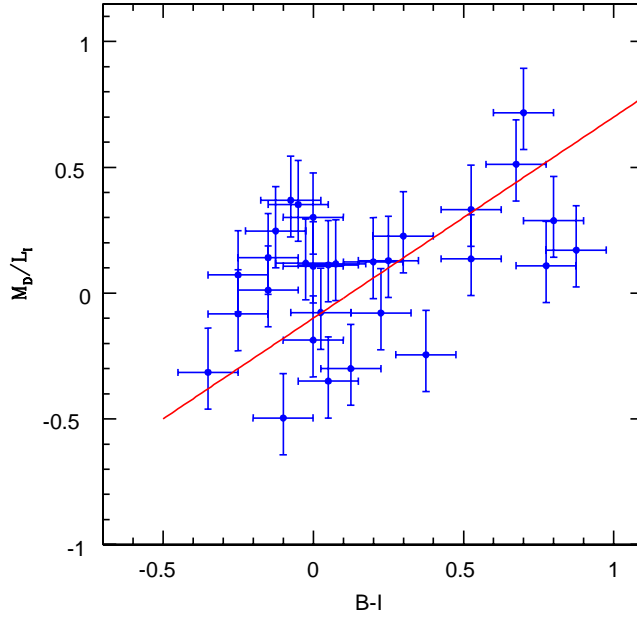


Fig. 3. Logarithm of the mass-to-light ratio in the I band as a function of the B-I color. The solid line is from Vazdekis et al. 1996. The uncertainty in B-I is 0.1 mag (Vazdekis et al 1996). In Fig.2 we show \mathcal{Y}_I vs. $B - I$ colors alongside with the same relation predicted by population synthesis models. We find

$$\mathcal{Y}_I \simeq 0.63 \times \left(\frac{1.6L_B}{L_I} \right)^2 \quad (3a)$$

in good agreement with Vazdekis et al. Finally, we compare the kinematical disk masses M_D with those derived from the galaxy spectro-photometry: $M_{phot} = \mathcal{Y}_I (B - I) L_I$ (let us remind that \mathcal{Y}_I is the average stellar mass-to-light ratio for a stellar population of color $B - I$). As a quite general outcome of the past history of galaxies, Vazdekis et al. 1996 found

$$\mathcal{Y}_I = b (B - I) + c \quad (3b)$$

where $b \sim 0.8$ and the value of the constant c is irrelevant. We find:

$$M_D = (0.96 \pm 0.1) M_{phot} \quad (4)$$

(28 d.o.f., see Fig 4), i.e. dynamical and photometric mass estimates statistically coincide. Notice that the disk mass and I-band luminosity are not directly proportional:

$$\log M_D = (0.79 \pm 0.1) \log L_I + const \quad (5)$$

with the log slope being significantly different from unity. Then, the existence of a relationship between the maximum rotation velocity and the galaxy luminosity is far from being a trivial one, in that the I-band luminosity is not a

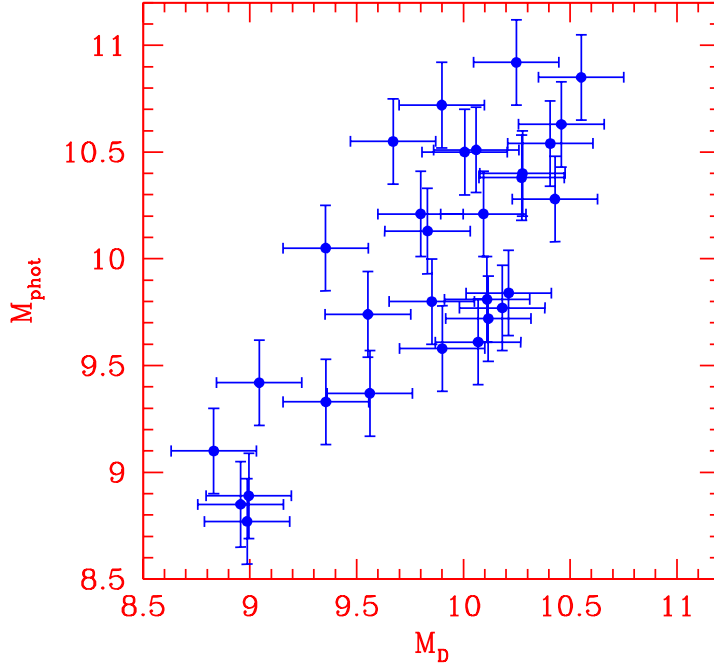


Fig. 4. Kinematical mass M_D vs photometric disk masses. Units in $\log M_\odot$

straightforward measure of the stellar mass. It is worth to note that in the 3-D space defined by the $(\log L_I, \log(M_D/L_I), B - I)$ coordinate vector, spirals are not randomly distributed, but occupy a very thin plane (see Fig. 2).

4 MDO/BH masses. Upper limits

The very good spatial resolution of the RC's of our sample plays a crucial role in the determination of strict and reliable MDO upper limits. In fact, since at small radii $V \propto R$ and the mass inside r_{in} scales as r_{in}^3 , a spatial resolution of $r_{in} \sim 100 pc$ yields to a mass resolution of $\sim 10^6 M_\odot$, given that $V(r_{in}) \sim 10 km/s$. In detail, the ratio of the rotational velocities $(V_{MDO}/V_d)^2 \propto (M_{MDO}/r_{in})^3$, implies that a higher spatial resolutions lead to stronger limits on M_{MDO} (or easier detection).

We now force the presence of a central MDO/BH by adopting the maximum possible MDO mass compatible with the rotation curve. We determine the upper mass limits by assuming $f = 1$ or $f = f_{max}$ with $f = f_{max}$ the value that brings the model RC 1σ higher than the innermost data. Note that for $f = 1$ all the mass inside r_{in} is in the black hole. We typically find: $f_{max} = 0.7 - 0.8$ and that, in spite of having an additional parameter, the disk+black hole model performs significantly worse than the OD model.

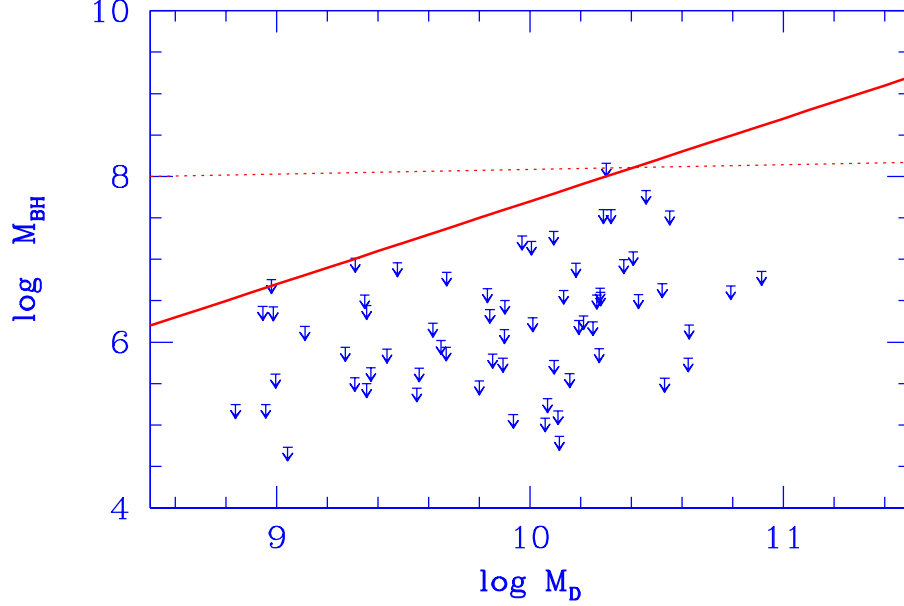


Fig. 5. Upper limits BH/MDO masses *vs.* disk masses. The solid line is the BH/MDO mass *vs.* stellar mass of ellipticals.

Notice that only in a few cases $f_{max} \sim 0.2$, furthermore, no result changes if we assume $f_{max} = 1$ for all the objects. M_{BH} is then obtained by substituting in equation (2b) the corresponding values of f . These are shown in Table 1: it is evident that typically $M_{MDO} \ll 10^8 M_\odot$ especially at low luminosity. It is clear that these limits are short of the mass residing in a accreting BH which is required to power high redshifts quasars, thus, spirals do not host QSO remnants (see also Salucci et al 2000). More specifically, if central MDO's of masses $\sim 2 M_{MDO}$ (and still $< 10^8 M_\odot$) were actually present at the center of the late type spirals of our sample, they would have affected the inner kpc of the available RC's more strongly than MDO's of $\sim 10^9 M_\odot$ affect the inner kinematics of ellipticals (Magorrian et al., 1998).

In Fig. 5 we show the relationship M_{BH} *vs.* the stellar disk mass M_D , and, as a reference, we plot the extrapolation to spirals of the elliptical's stellar mass-MDO/BH mass relationship $M_{MDO} = 0.005 \times M_{stars}$ (Magorrian et al., 1998, Kormendy & Richstone 1995). We immediately realize, that in spirals, the MDO masses, if different from zero, are however much smaller than those detected at the centers of ellipticals of same stellar luminosity; whether this is related to their less prominent bulge content or does reflect also a morphological mass segregation, will be considered elsewhere (Salucci et al 2000). Notice that in the same paper we perform a detailed investigation on possible biases occurring in the present estimate of the MDO upper limits.

5 DISCUSSION

Accurate mass models of the innermost kpc of 83 spirals derived from high spatial resolution RC's, reveal that, inside this region, the luminous matter fully accounts for the observed kinematics: a stellar disk of constant mass-to-light ratio (in some cases in conjunction with a spheroid) is virtually the only mass component. In this region, with the exception of very high luminosity galaxy with complex dynamics, we find

$$V^2(R) \propto \text{light}(< R)/R \quad (6)$$

which is indicative of the absence of a sizable dark component. Therefore, the only possibility for the presence of a dark halo in the central regions of spirals is that it conceals itself below the detection threshold.

More in detail, inside the innermost kpc or so, the contribution to the gravitational potential from a dark component cannot exceed 10%; this is in disagreement with claims and scenarios in which a dark halo has a major role at any radii. Moreover, in the same objects studied here, the DM, undetected at $R < 1/3 R_D$, begins to dominate the mass distribution at $R \sim 3R_D$ (PSS). Then, the dark mass inside a given radius R must increase with R very steeply, e.g. as in the case of a constant density distribution.

In a DM-free environment, we have been able to estimate the disk masses also for objects in which the global influence of the dark matter is relevant and to relate disk colors and masses across a large range of galaxy luminosities. The next step will be to pursue a coordinated kinematical and photometric study to tackle open cosmological issues.

6 Appendix

In the appendix we produce the two Tables of galaxy and MDO/BH properties.

References

- [1] Ghez A.M, Cline B.L, Morris M., Becklin E.E., 1999, ApJ 509, 678
- [2] Genzel R., AAS, 1998, 193, 620
- [3] Ho L.C., 1998, in *Observational Evidence for Black Holes in the Universe*, ed. Chakrabarti, S. K., Kluwer Academic Pub.
- [4] Kormendy J., Richstone D., 1995, ARA&A, 33, 581
- [5] Magorrian J., Tremaine S., Richstone D., Bender R., Bower G., Dressler A., Faber S.M., Gebhardt K., Green R., Grillmair C., Kormendy J., Lauer T.R., 1998, 115, 2285
- [6] Persic M., Salucci P., 1995 (PS95), ApJS, 99, 501
- [7] Persic M., Salucci P., 1990, MNRAS, 245, 577
- [8] Persic M., Salucci P., Stel F. (PSS), 1996, MNRAS, 281, 27
- [9] Rhee M.H. 1997, Phd. Thesis, Groningen University
- [10] Salucci P., Persic M., A&A, 351, 442
- [11] Salucci P., Ratnam C., Monaco P., Danese G., 2000 MNRAS in press
- [12] Salucci P., Szuszkiewicz E., Monaco P., Danese G., 1999 MNRAS, 307, 637
- [13] Vazdekis A., Casuso E., Peletier R.F., Beckman J.E., 1996, ApJS, 106, 307
- [14] Vazdekis A., Peletier R.F., Beckman J.E., Casuso E., 1997, ApJS, 111, 203

<i>name</i>	M_D	B-I	\mathcal{Y}	L_I
116-G12	9.83	.675	.51	9.59
121-G6	10.27	.700	.72	9.84
143-G10	8.83	.225	-.08	8.92
346-G26	10.11	-.125	.247	9.82
347-G28	9.56	-.150	.01	9.49
347-G33	10.40	.300	.23	10.30
347-G34	10.27	.025	-.08	10.36
357-G16	8.99	-.350	-.32	9.17
359-G6	9.04	-.100	-.5	9.50
362-G11	9.89	.775	.11	10.10
374-G8	8.95	.000	.11	8.85
380-G23	9.67	.875	.17	9.85
406-G26	10.11	.000	.30	9.81
418-G1	9.85	.050	.11	9.76
441-G2	10.18	-.050	.35	9.81
468-G23	9.55	.000	-.19	9.74
487-G2	10.00	.525	.14	10.08
488-G54	10.21	-.250	.07	10.04
51-G18	10.06	-.075	.37	9.67
533-G53	10.06	.125	-.30	10.41
54-G21	9.35	.375	-.25	9.75
554-G28	9.35	.075	.12	9.27
556-G23	10.09	.200	.12	10.05
566-G22	9.90	-.150	.14	9.70
60-G25	8.98	-.250	-.08	8.97
84-G10	9.80	.050	-.35	10.17
305-G6	10.45	.250	.13	10.43
476-G15	10.42	-.025	.12	10.30
79-G14	10.55	.525	.33	10.43
79-G3	10.24	.800	.29	10.28

Table 1

(1) Galaxy name (2) Logarithm of the disk mass in solar units (3) B-I color (4) Logarithm of the disk mass-to-light ratio (I-band). (5) I-Band luminosity.

<i>name</i>	<i>logM_{BH}</i>	<i>name</i>	<i>logM_{BH}</i>	<i>name</i>	<i>log M_{BH}</i>
116-g12	6.6	418-g8	6.4	m-1-2524	7.0
121-g6	6.7	436-g3	6.7	m-214003	6.3
13-g16	5.9	441-g2	7.0	m-3-1042	5.8
143-g10	5.2	446-g53	6.8	n1090	5.6
157-g20	7.2	468-g23	5.4	n1832	8.3
157-g38	5.9	481-g13	5.6	n2763	7.6
162-g17	6.2	487-g2	7.2	n3715	8.2
233-g42	6.3	488-g54	6.3	n4348	6.2
249-g16	5.8	490-g28	5.9	n699	6.3
249-g35	5.5	490-g45	7.3	n7218	7.6
265-g2	6.7	498-g3	6.6	n7339	6.6
302-g9	6.6	51-g18	5.3	n755	5.7
328-g43	6.2	533-g53	5.1	ua17	5.8
329-g7	7.2	54-g21	5.5	269-g19	8.3
346-g26	4.9	545-g3	5.1	305-g6	7.8
347-g28	5.7	545-g5	6.4	358-g63	6.7
347-g33	7.1	547-g24	7.0	36-g19	7.7
347-g34	5.9	55-g4	6.3	476-g15	6.6
35-g18	7.7	550-g7	5.6	545-g11	8.3
357-g16	5.6	554-g28	6.4	547-g31	7.4
359-g6	4.7	556-g23	7.3	582-g12	7.7
362-g11	6.2	563-g14	7.3	79-g14	7.6
374-g8	5.2	566-g22	6.5	79-g3	6.2
380-g23	6.8	575-g53	6.0	i96099	6.9
406-g26	5.2	58-g30	6.6	m-222025	8.6
410-g19	7.0	60-g25	6.4	n4705	7.2
418-g1	5.9	84-g10	5.5	n697	8.4
I407	7.	I96099	6.9		

Table 2

BH/MDO upper limits for the galaxies of the sample, in units of $\log M_{\odot}$